Energy 298 (2024) 131306

Contents lists available at ScienceDirect

Energy

journal homepage: www.elsevier.com/locate/energy

Numerical simulation of the co-firing of pulverized coal and eucalyptus wood in a 1000MWth opposed wall-fired boiler

Junxuan Huang [a], Yanfen Liao [a,*], Jianhua Lin [b], Changjiang Dou [b], Zengxiu Huang [b], Xiongwei Yu [b], Zhaosheng Yu [a], Chunxiang Chen [c], Xiaoqian Ma [a]

[a] Guangdong Province Key Laboratory of Efficient and Clean Energy Utilization, School of Electric Power, South China University of Technology, Guangdong, Guangzhou, 510640, China
[b] China Resources Power (Hezhou) Co., Ltd, Hezhou City, 542700, China
[c] College of Mechanical Engineering, Guangxi University, University Road 100, Xixiangtang District, Nanning City, 530004, China

ARTICLE INFO

Handling editor: Krzysztof (K.J.) Ptasinski

Keywords:
Opposed firing boiler
Co-firing of biomass,NO_x reduction
Air-staged combustion
Numerical simulation

ABSTRACT

Currently, coal-fired coupled biomass power generation is widely regarded as a primary method for reducing carbon emissions in coal-fired power plants. This research investigates the co-firing of biomass in an opposed wall-fired boiler and the implementation of air-staged combustion technology using numerical simulation approaches. The study examines the impact of various air methods of distribution and blending ratios on combustion properties and NO_x emissions. The findings demonstrate that the abrasive wear of fuel particles on the platen superheater is decreased by the addition of biomass to the fuel mix. Furthermore, a drop in the furnace chamber's overall temperature is the outcome of raising the blending ratio. Different blending ratios have their own adapted air distribution methods. At blending ratios of 10% and 30%, the W-type air distribution exhibits the lowest NO_x outlet concentrations of 231.84 mg/Nm^3 and 220.6 mg/Nm^3, respectively. Moreover, the W-type air distribution shows the highest burnup rates of 98.74% and 98.43% at these blending ratios. This suggests that it is feasible to change the burner monolayer air distribution and combine it with co-firing of biomass technology to achieve low NO_x and efficient operation of a hedge-fired boiler.

Nomenclature

NO_x	Nitrogen Oxides
PA	Primary Air
SA	Secondary Air
OFA	Over-Fired Air
SCR	Selective Catalytic Reduction
CFD	Computational Fluid Dynamics
DPM	Discrete Phase Model
LHV	Low Heating Value
PC	Pulverized Coal
EW	Eucalyptus Wood
RANS	Reynolds Averaged Numerical Simulation
WSGGM	Weighted Sum of Gases Model
BMCR	Boiler Maximum Continuous Rating
Symbols	
m_p	particle mass [kg]
$\vec{v}$	velocity vector [m/s]
$\vec{F}$	composite force [kg·m/s]
$C_{p,P}$	specific heat
Q_C	convective heat
Q_r	radiant heat
R_1, R_2	competing rates
A_1, A_2	rate constants [−]
E_1, E_2	combustion reaction rate constants [−]
$m_v(t)$	volatility rate of over time [%]
$f_{W,0}$	mass fraction of substance evaporated [%]
$m_{p,0}$	initial particle mass [kg]
α_1, α_2	yield factors [−]
m_a	ash content [%]
A_P	surface area of particles [m^2/kg]
P_{ox}	partial pressure of oxidizer [Pa]
D_0	diffusion rate [m^2/s]
d_P	particle diameter [m or μm]
$\mathscr{R}$	universal gas constant [−]
f	fuel mixing fraction [−]
Z_i	mass fraction of elements [−]

* Corresponding author.
E-mail address: yfliao@scut.edu.cn (Y. Liao).

https://doi.org/10.1016/j.energy.2024.131306
Received 8 November 2023; Received in revised form 3 April 2024; Accepted 12 April 2024
Available online 17 April 2024

1. Introduction

In light of the swift progress of industrialization and societal advancements, there is a growing awareness and emphasis on environmental concerns. According to the IPCC report [1],anthropogenic warming will reach 1.26 °C in 2022, the global warming rate is accelerating and has surpassed 0.2 °C every ten years. Biomass fuels possess significant potential for mitigating emissions of carbon footprint, nitrogen oxides, and other pollutants, and have long been acknowledged as a valuable and sustainable source of energy [2]. However, due to the limitations of biomass production, transportation conditions and combustion technology [3,4], the technology of large-scale utilization of biomass is still at the stage of exploration.

The development of co-firing of biomass technology provides a good idea to solve this problem. In previous years, numerous researchers have extensively studied the feasibility and adaptability of co-firing biomass in coal-fired boilers [5,6]. Oladejo et al. [7] found that by co-firing Yunnan coal with oat straw and rice hulls at a biomass mixing ratio of 30 wt%, a significant synergistic effect was observed on the organic content and ash catalytic activity of the coal. Wu et al. [8] experimented with co-combustion of bituminous coal and corn stover and found that the release of mineral elements was reduced as the percentage of corn stover increased. Additionally, they observed that the liberation of alkali metals was enhanced with increasing temperature and percentage of corn stover. Tu et al. [9] examined the impact of wheat straw blending position on NO_x emissions in a coal-fired tangential furnace. The findings revealed that incorporating biomass at the upper level resulted in a temperature field resembling that of pure pulverized coal combustion, thereby leading to the lowest NO_x emissions. A numerical simulation investigation of co-firing biomass in a 500 MWe coal-fired power station was carried out by Mun et al. [10]. The results demonstrated that the boiler efficiency was significantly impacted by both the amount of moisture and the calorie density of the biomass employed as a co-firing fuel. It was also discovered that in order to get the maximum boiler efficiency, roasting raises the fuel's calorific value and grindability.

To control the emission of nitrogen oxides in coal-fired power plants, many low-NO_x combustion technologies are widely adopted. Selective Catalytic Reduction (SCR) technology is considered the most efficient method for removing NOx in coal-fired power plants. However, the cost of catalysts and reducing agents used in SCR technology is relatively high. Additionally, catalyst deactivation can occur due to factors such as high-temperature sintering, blockage [11], alkali poisoning, and acid poisoning [12]. The recycling and regeneration of discarded SCR catalysts also pose significant challenges. Swirl burners, as efficient and low-emission combustion devices, have been a hot topic in the research of low-NO_x combustion. Many scholars have optimized the dimensions and structures of the burner's air ducts and applied them in opposed wall-firing boilers [13]. Oxygen-enriched combustion aims to use pure oxygen or O_2/CO_2 as the oxidant for combustion. This technique is widely applied in coal-fired power plants and waste incineration plants [14,15]. During oxygen-enriched combustion, increasing the concentration of O_2 can effectively suppresses the formation of fuel NO_x and thermal NO_x [16]. Additionally, coupling with flue gas recirculation technology can significantly reduce NO_x emissions [17].

The air-staged combustion technology is one of the most declaring low-NO_x combustion technologies available. The main combustion zone, reduction zone, and combustion zone are formed in the furnace chamber by effectively managing the local excess air coefficient in the combustion chamber. This may successfully boosts the rate of combustion of pulverized coal and lower NO_x emissions. The study conducted by Wang et al. [18] focused on exploring the impact of multiple air staged combustion on both the rate of pulverized coal combustion and the characteristics of nitrogen oxide (NO_x) emissions. The experiments were carried out using a one-dimensional pulverized coal combustion experimental furnace system, with the total air volume kept constant. The findings of the study indicated that the implementation of three-stage air staged combustion led to a notable reduction in NO_x emissions compared to single air staged combustion. Specifically, the NO_x emission level decreased from 729.8 mg/m^3 under single air staged combustion to 534.5 mg/m^3 under three-stage air staged combustion. This suggested that multiple air staged combustion had the potential to effectively mitigate NOx emissions during pulverized coal combustion processes. The results supported the notion that optimizing the air staging strategy can contribute to the reduction of NO_x emissions. They also conducted numerical simulations on an existing 600 MW coal-fired boiler [19]. The simulations compared shallow air-staged combustion ($\alpha M = 0.95$) and deep air-staged combustion ($\alpha M = 0.75$) at the exit of the furnace, with the aim of achieving a final NO_x reduction efficiency of 31.6%. Sung et al. [20] aimed to evaluate the combustion performance of air-staged for different pulverized coal fineness levels in a laboratory-scale pulverized coal furnace. The focus was specifically on investigating the effect of air staging on nitrogen oxide (NO) emissions

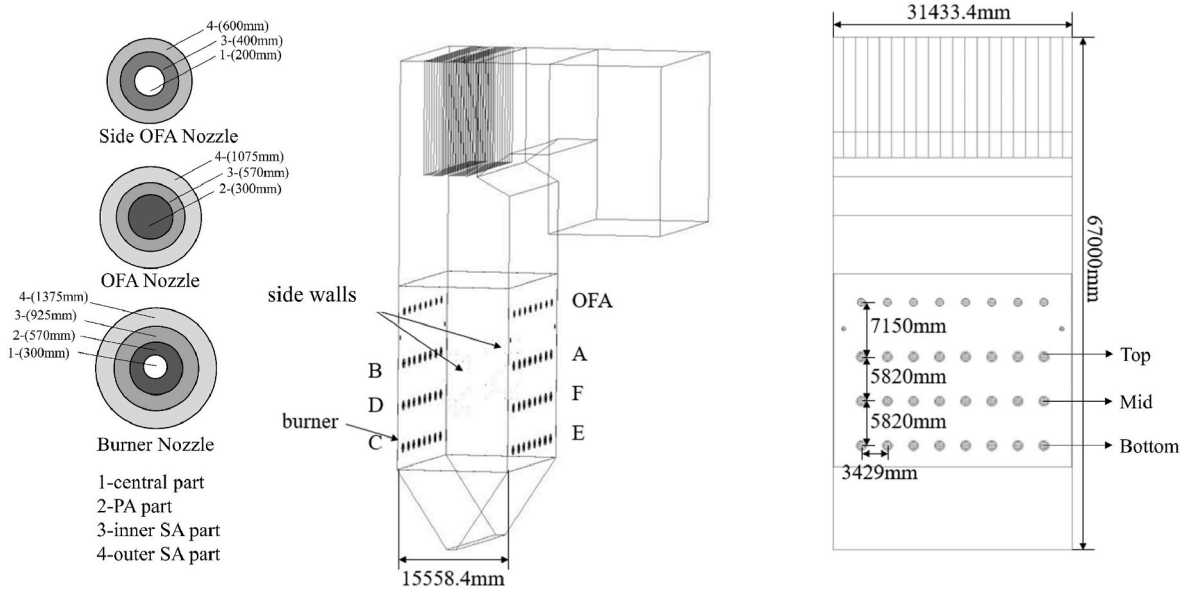

Fig. 1. Schematic diagram of boiler structure.

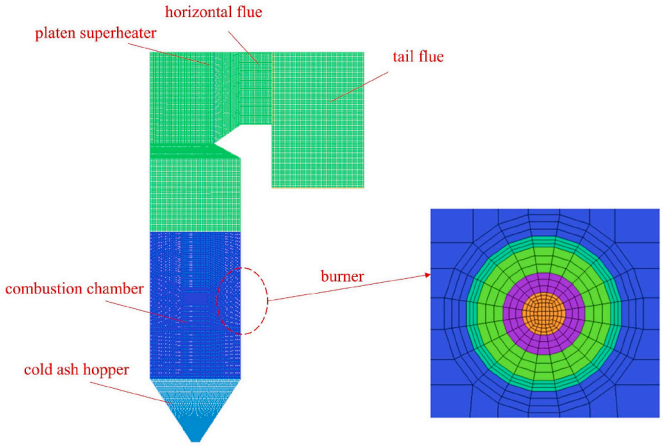

Fig. 2. Mesh scheme applied to the boiler.

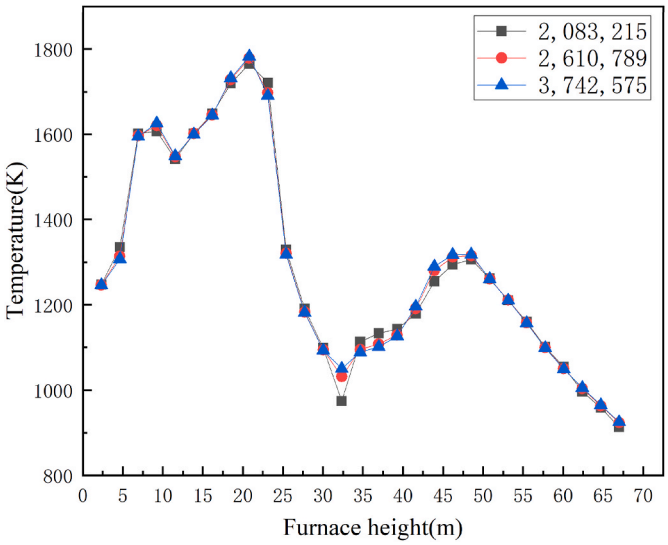

Fig. 3. Mesh independence verification.

during pulverized coal combustion. The researchers observed that, within the average particle size range of 50–120 μm, air-staged combustion had minimal impact on NO emissions from pulverized coal combustion. This suggested that, for this particular particle size range, altering the air staging strategy did not result in significant changes in NO emissions. However, there was a direct relationship between NO emissions and the average particle size range of 45–125 μm in the non-air-staged case. For opposed wall-fired equipment, NO and CO are usually a contradiction in terms. It is common that the distribution of CO concentration along the width of the furnace is low in the middle and high on both sides, with unsatisfactory combustion uniformity and CO enrichment on the side walls [21]. In conclusion, research on air-graded combustion technology and biomass blending technology for large-scale units is a current priority.

Current research on biomass blending in pulverized coal boilers mainly focuses on the burnout rate of the fuel mixture and the effect of boiler efficiency. Few studies have examined the effect of the same layer of air distribution on the NO_x emissions from biomass blending. Based on CFD technology, we carried out numerical simulations of single-layer air distribution and biomass blending technology in a coal-fired boiler to explore effective methods for boiler operation with high efficiency and low pollution. The research conducted in this paper focused on a 1000MWth opposed wall-fired boiler. We explored the boiler operating conditions in the form of interacting variables for different air distribution methods and biomass blending ratios. The interaction of these two variables was explored by comparing the temperature field, burnout rate and pollutant emission concentration. Finally, the advantages and disadvantages of various air distribution methods with different blending ratios were evaluated by considering all the simulated working conditions. The purpose of this study is to provide a reference for lowering NO_x emissions and to explore the possibility of combining air-staged combustion technology with blending combustion technology to enhance the nitrogen reduction performance and combustion efficiency of coal-fired boilers.

2. Mathematical models and methods

2.1. Research subjects

The Simulation Power Plant Boiler is an ultra-supercritical opposed wall-fired boiler with a capacity of 1000 MWth manufactured by Dongfang Boiler Co. The boiler is arranged in a Π-shape with a width of 31433.4 mm, a depth of 15558.4 mm and a height of 67000 mm. In order to simplify the boiler, the model is divided into cold ash hopper, combustion chamber, platen superheater section, horizontal flue, and tail flue section, and the detailed structure is shown in Fig. 1. Where the platen superheater section is involved in heat transfer and particle collision calculations in the gas flow. There are 48 swirl burners in the combustion chamber section, which are arranged on three levels in the front and back walls. The #A and #B tier burners are named the Top section, the #D and #F tier burners are named the Mid burners, and the #C and #E tier burners are named the Bottom burners. The top of the combustion chamber is arranged with 20 over fire air inlets named OFA layer, and 4 side over fire air inlets are also arranged against the side wall part.

Numerical simulation of power station boiler was carried out using commercial software FLUENT. The boiler model was firstly meshed and the burner section was locally encrypted. Due to the presence of numerous pipes and heat exchangers in the actual boiler, the platen superheater and the overall boiler flow path were retained in order to simplify the model and not lose generality. The overall details of the grid model are shown in Fig. 2. The network was tested independently and the average temperature along the furnace height section was selected as the comparison criterion. The number of comparison grids were 2,083,215, 2,610,789, and 3,742,575, and the results are shown in Fig. 3, where the temperature error for each number of grids is within ±5%, indicating that 2,610,789 grids have achieved the accuracy of the simulation.

2.2. Reaction models

All the physical models used in this paper have been widely used in the simulation of power station boilers. In general, CFD-based blending combustion models generally include particle phase combustion models, gas phase models and NOx model. The reaction and motion processes of the fuel inside the boiler were usually described by a discrete particle model (DPM) with steady-state tracking of the particles. The Rosin-Rammler distribution was used to characterize the particle size distribution [22]. In this study, in order to better predict the flame of swirl combustor, a realizable k-ε model that is more suitable to be used in the case of higher turbulence intensity was adopted [23]. The radiation model was based on the P1 model [24] and the weighted-sum-of-gray-gases model (WSGGM) was used to describe the gas emissivity. The SIMPLE model was used as the pressure-velocity coupling model solver. The gradient of spatial discretization was described using the Least Squares Cell Based method. The detailed modeling equations are presented in the Supplementary Material.

NO_x is a major pollutant in power station boiler exhaust emissions, especially NO. NO_x production is categorized into the following three main types: fuel NO_x, thermal NO_x, and prompt NO_x. Prompt NO_x is

Table 1
Proximate and ultimate analysis of fuel.

Samples	Proximate analysis (as received basis, wt. %)				Ultimate analysis (dry ash basis, wt. %)					LHV kJ/kg
	Volatiles	Fixed carbon	Ash	Moisture	C	H	O	N	S	
EW	60.96	14.45	13.23	11.36	42.07	5.16	37.02	0.82	0	17,260
PC	28.35	47.43	15.09	9.13	62.45	3.91	14.98	1.47	0.58	28,490

Table 2
Main parameters of each working condition.

Case	Coal consumption rate (kg/s)	Biomass consumption rate (kg/s)	Blending ratio (%)	Co-firing position	Air distribution
#0 (basic case)	106.03	0	–	\	U
#1	95.43	10.60	10	A3/A6/B3/B6	U
#2	84.82	21.21	20	A3/A6/B3/B6/D3/D6/F3/F6	U
#3	74.22	31.81	30	A3/A6/B3/B6/C3/C6/D3/D6/E3/E6/F3/F6	U
#4	95.43	10.60	10	A3/A6/B3/B6	I
#5	84.82	21.21	20	A3/A6/B3/B6/D3/D6/F3/F6	I
#6	74.22	31.81	30	A3/A6/B3/B6/C3/C6/D3/D6/E3/E6/F3/F6	I
#7	95.43	10.60	10	A3/A6/B3/B6	W
#8	84.82	21.21	20	A3/A6/B3/B6/D3/D6/F3/F6	W
#9	74.22	31.81	30	A3/A6/B3/B6/C3/C6/D3/D6/E3/E6/F3/F6	W

mainly due to the reaction of hydrocarbons in the fuel with N_2 molecules in the air to form CN and HCN, which are then oxidized to NO_x [25]. Generally for power station boilers when the excess air coefficient is large, such NO_x generation is less, so in this paper only the effect of the first two NO_x is considered. The detailed NO_x generation modeling equations are presented in the Supplementary Material.

Considering that the generation of NO_x has little influence on the temperature field and component field. In this paper, the calculation method of post-processing was adopted, based on the steady state temperature field obtained from the previous calculation before the calculation of NO_x. This can ensure the accuracy of the calculation and also speed up the calculation speed.

2.3. Simulation conditions

The boiler conditions studied in this paper were based on the BMCR combustion condition, with an outlet steam volume of 3033.00 t/h and a fuel input of about 381.71 t/h. The fuels used were Indonesian lignite and eucalyptus. The proximate analysis, ultimate analysis, and low heating value (LHV) of the two fuels are shown in Table 1. The total excess air factor was taken as 1.1 and air was injected from each inlet of the burner. The center air, primary air, and inner secondary air were injected in a direct current, and the outer secondary air was injected into the flow field as a cyclone. Eucalyptus wood used in the actual power plant is crushed and ground using a crusher. For blending conditions, blending ratios of 10%, 20%, and 30% were selected, with each burner combusting only one type of fuel individually. Both pulverized coal and eucalyptus wood particle size followed Rosin-Rammler distribution with minimum diameter of 0.001 mm, maximum diameter of 0.2 mm. The average diameter of pulverized coal is 0.07 mm and eucalyptus wood 0.18 mm. The spread parameter is 4.52 and number of diameters is 10. The detailed boundary conditions are shown in Table 2.

In this paper, the actual power plant boiler regulated the air intake of each burner by valve openings. The burner near the side wall had a higher air intake, and the valve opening became smaller towards the center of the combustion chamber. The valve openings of the burners in the same layer from #1 to #4 were 90%, 70%, 50%, 40% and vice versa for #5 to #8. The inlet air volume on the same side formed a U-shape, naming this air distribution method as U-type air distribution. Similarly, we named the case where each burner valve opening was the same on the same side as I-type air distribution, and the case where the burner valve openings were adjusted to 70% and 30% and arranged alternately as W-type air distribution. The detailed diagram of air distribution is presented in the Supplementary Material (Fig. S1). The above three air distribution methods will be discussed one by one in Chapter III. Also, in order to minimize the effect of uneven heat flow density distribution in each section of the furnace after blending, the eucalyptus settings were fed from different burners for different blending ratios.

Table 3
The comparison of measured and simulated data of the outlet parameters.

Parameters	Simulated data	Measured data	Relative error
Temperature(K)	1283.17	1351.79	−5.08%
CO concentration (mg/Nm_3)	10.24	10.88	−5.88
NOx concentration (mg/Nm_3)	246.48	254.10	−2.99%

3. Results and discussion

3.1. Model validation

In order to check the accuracy of the model, it was necessary to compare the simulation results with the field measurement data of the pulverized coal furnace. The BMCR working condition boundary condition was selected for simulation and named case#0. Three parameters, temperature, oxygen content and SO_2 concentration of the outlet cross section were selected for examination. The measured plane was the actual boiler low temperature reheater outlet, which was used as the outlet for the simulation. The data were taken from the steady state conditions of the actual power plant over a period of time with an interval of 10 min and the average of the selected data was taken and the results of the comparison are shown in Table 3. The error results for all three parameters were within 10%, and the simulation results could be considered to be in line with the accuracy.

3.2. Co-combustion of biomass at different ratios

3.2.1. Velocity flow field distribution

Fig. 4 shows the velocity cross-section contours of the uppermost layer for different eucalyptus mixing ratios in the U-type air distribution method. From the figure, it can be observed that the air flow decreases gradually from the left and right walls towards the center as the valve opening changes. A low velocity zone is formed in the center, which increases the duration of fuel particles in the combustion chamber and effectively improves the combustion efficiency. There is no significant

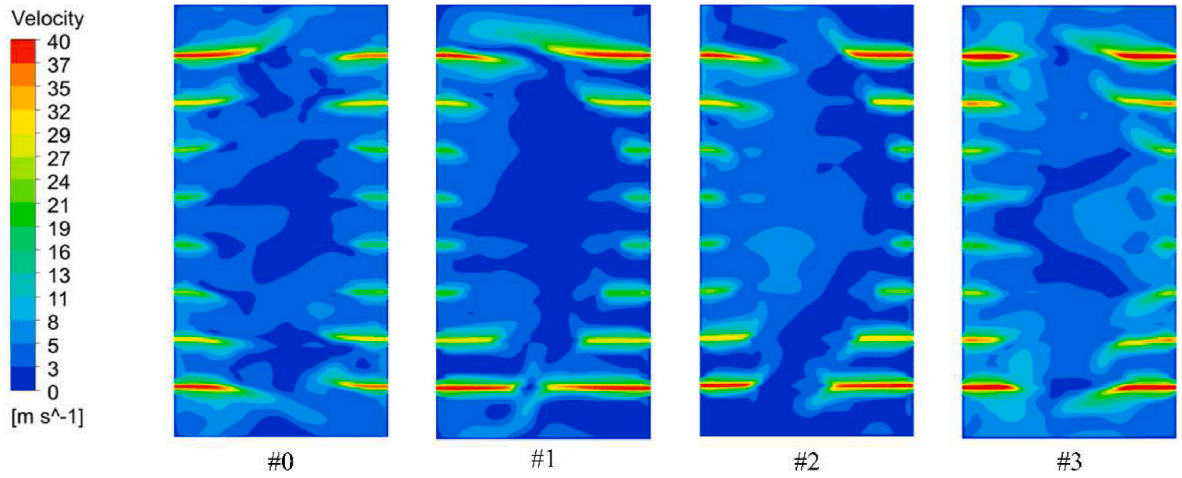

Fig. 4. Velocity distribution of the top burner.

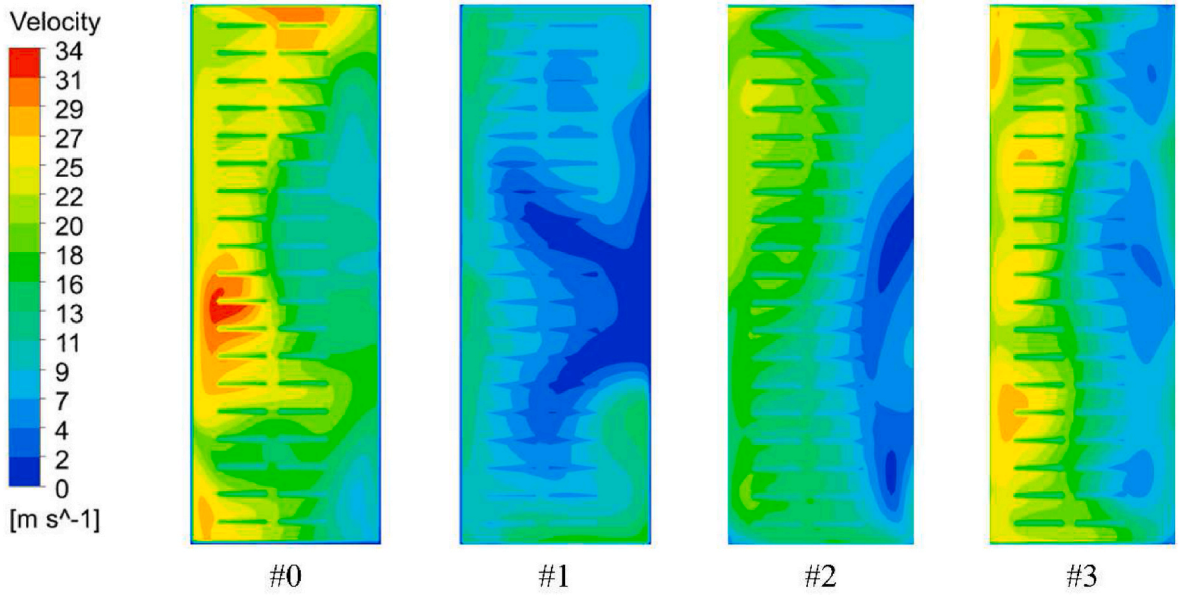

Fig. 5. Contours of velocity of the platen superheater.

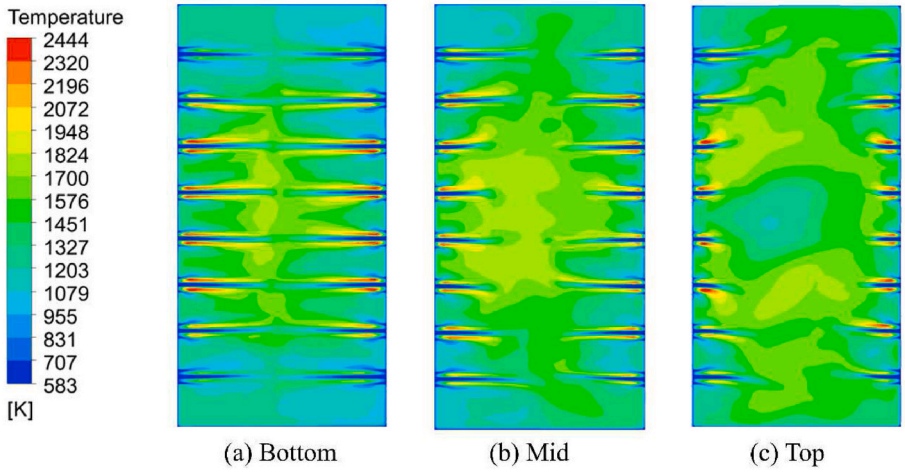

Fig. 6. Temperature distribution in different layers of the burner in case #0.

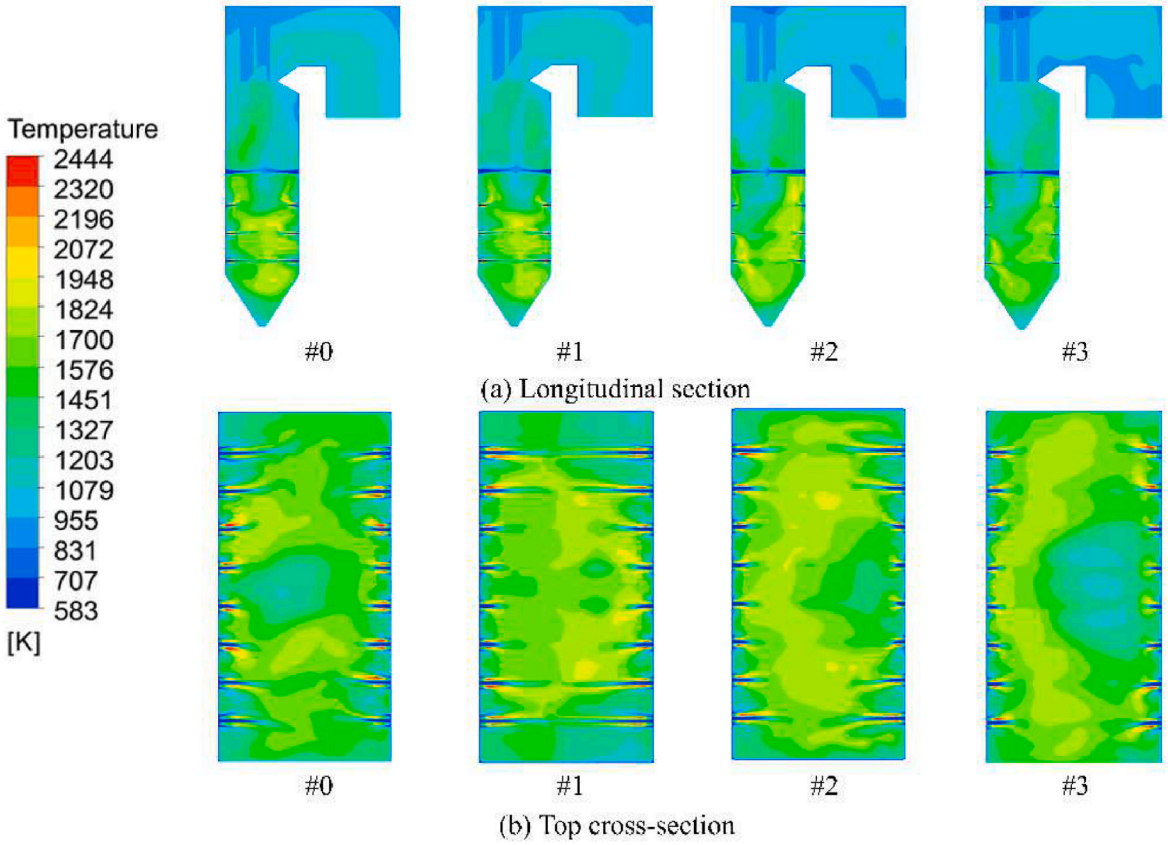

Fig. 7. Temperature distribution for different blended cases.

change in the velocity flow field as the blending ratio increases, which is consistent with the results of Li et al. [26]. However, it is interesting to note that by comparing the outlet cross-sectional velocities of the boiler, we find that the velocity slows down after blending the biomass. The exit cross-sectional velocities of case#1, case#2, case#3, and case#4 are 13.61 m/s, 9.05 m/s, 10.68 m/s, and 11.06 m/s, respectively. The decreased gas flow rate reduces the degree of fly ash scouring of the boiler and reduces fly ash corrosion of the heated surfaces. It can be observed through Fig. 5, comparing the airflow velocity in the area of the platen superheater, the blending ratio of 10% particulate matter scouring velocity is the slowest, and the increase of the blending ratio will increase the airflow velocity, but the degree of scouring is smaller than the pure pulverized coal condition in the case of the ratio of 30% or less, and there is a better ability to prevent the abrasion.

3.2.2. *Temperature flow field distribution*

The temperature distribution of the flow field is an important indicator for evaluating the economy, safety and environmental friendliness of power station boilers. Fig. 6 illustrates the temperature distribution contours for three different combustion layers of a pure pulverized coal combustion boiler with U-type air distribution under BMCR operating conditions. Due to the high air supply from the left and right side walls, a U-shaped front-like surface is formed on both sides of the flame, creating a high-temperature zone in the center area. The concentration of high-temperature areas is conducive to reducing the phenomenon of wall-attached combustion on both sides and reducing the high-temperature corrosion of the water wall [27]. As observed, in the Bottom layer of the combustion chamber, the airflow rigidity is higher, and the high-temperature zone of the flame is closer to the centerline. However, in the Mid and Top layers, due to the upward flow of the lower airflow, the flame length is further shortened, and the high-temperature zone of the flame gradually shifts towards the sides. This phenomenon is consistent with the study of Wang [19] et al.

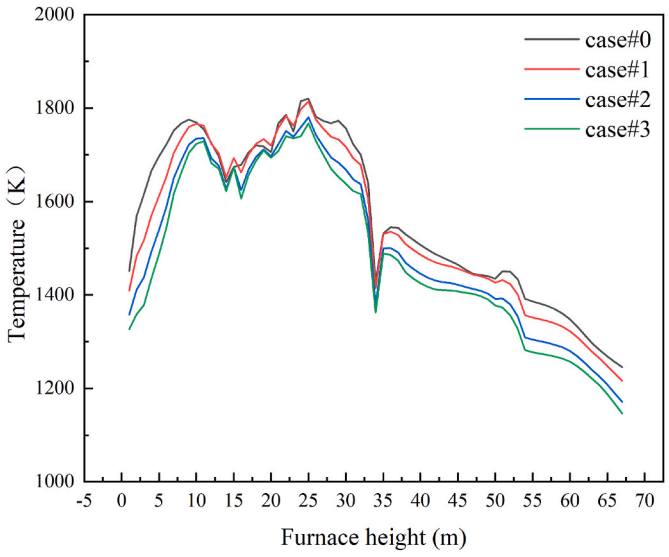

Fig. 8. Temperature distribution along the furnance height under U-type air distribution for different blended cases.

The temperature distribution for the U-type air distribution case with different blending ratios is shown in Fig. 7. Eucalyptus wood has a higher volatile content, which results in faster particle combustion rate when injected into the furnace. It also has an earlier ignition point compared to pure coal powder combustion. This leads to a more uniform distribution of flames and a larger coverage area of the high-temperature zone compared to pure coal powder combustion. The

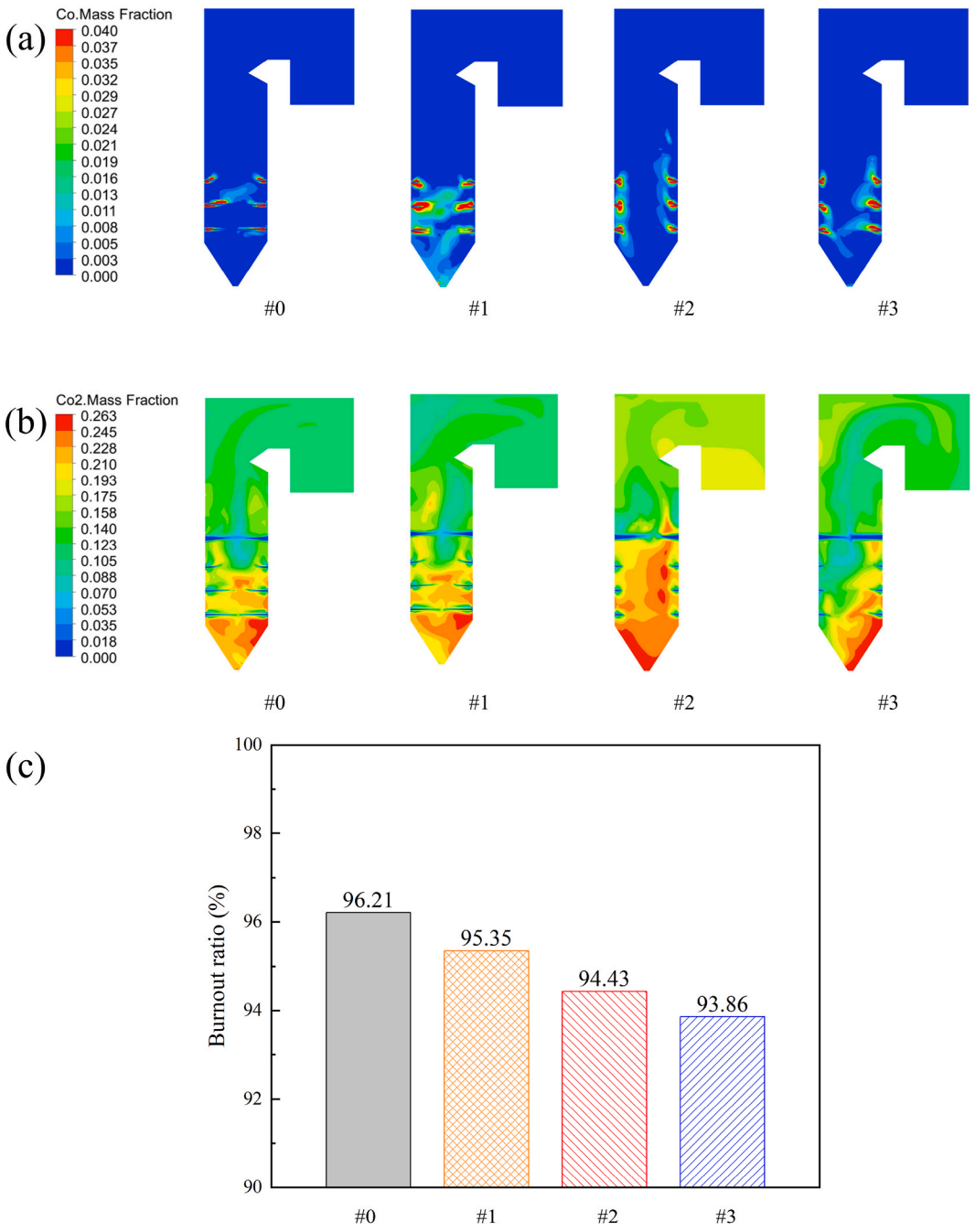

Fig. 9. Carbon monoxide (a) and carbon dioxide (b) concentration distribution for different blended cases; (c) Burnout ratio for different blended cases.

distribution of furnace temperature along the height for different blending ratios is given in Fig. 8. As the proportion of eucalyptus wood mixing increases, the temperature in the furnace region (height = 13–26 m) gradually decreases, and the temperature difference is more significant in the upper region of the over-fired air (height = 33–50 m).

3.2.3. *Component flow field distribution*

The conversion pathway of carbon elements is a research topic of significant interest in industrial combustion. As shown in Fig. 10, in case #1, a higher CO mass fraction is observed in the center of the furnace compared to the pure coal powder combustion condition. This is because CO primarily originates from the devolatilization process of the fuel [28], and biomass has a higher volatile content than coal powder. Consequently, the CO concentration is higher at the fuel inlet. The CO concentration gradually decreases with the increase of blending amount, but is still higher than the pure pulverized coal combustion condition (case#0). Biomass combustion increases the CO concentration to form a reducing atmosphere, which is favorable for suppressing the formation of NO_x.The high CO_2 content area is mainly concentrated in the high temperature zone of combustion, including the carbon in the fuel and the redox reaction of CO and oxygen produced by the reaction [29]. In the lower part of the furnace, the further combustion of residual carbon will also lead to a localized increase in CO_2 concentration. The addition of biomass will have varying degrees of impact on the combustion efficiency inside the furnace. As can be seen from Fig. 9(c), before the co-firing with biomass, the coal powder has the highest burnout rate, reaching 96.21%. However, after adding biomass, the overall burnout rate of the fuel decreases to some extent. Further increasing the blending ratio, the burnout rate decreases as the blending ratio increases. 30% blending ratio reduces the burnout rate by 2.35% compared to the #0

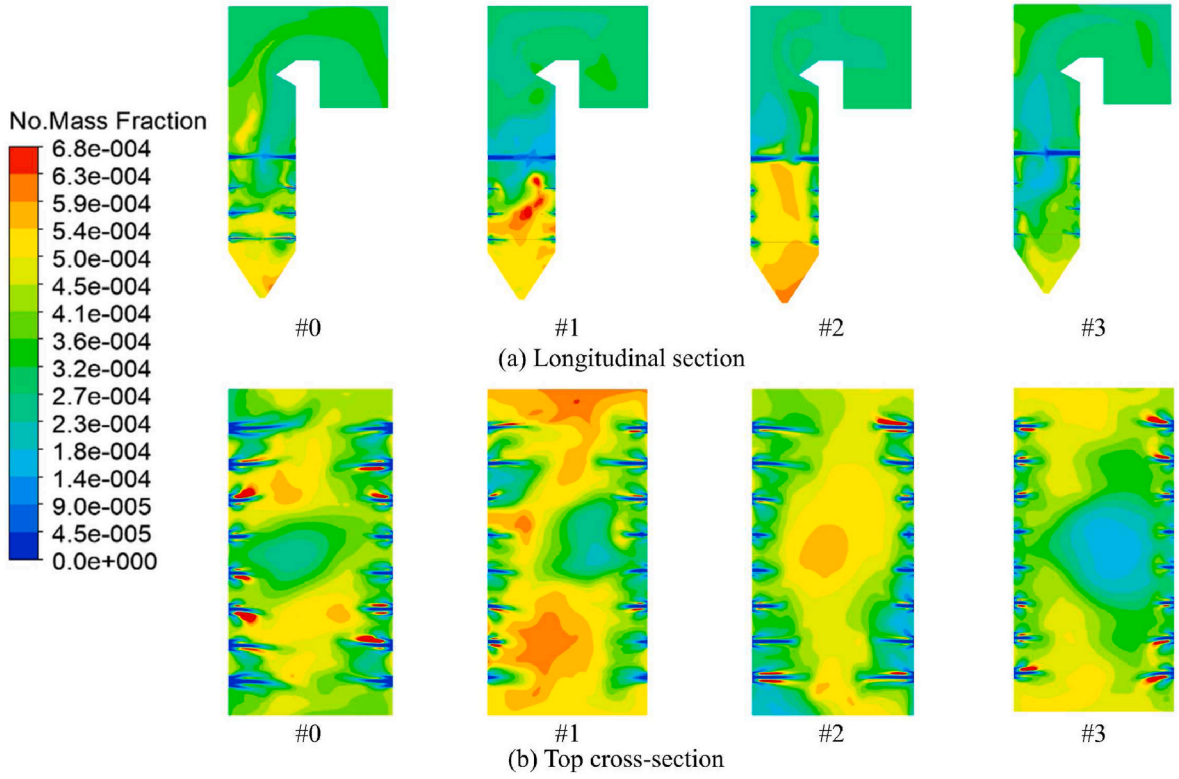

Fig. 10. NO_x concentration distribution under U-type air distribution for different blended cases.

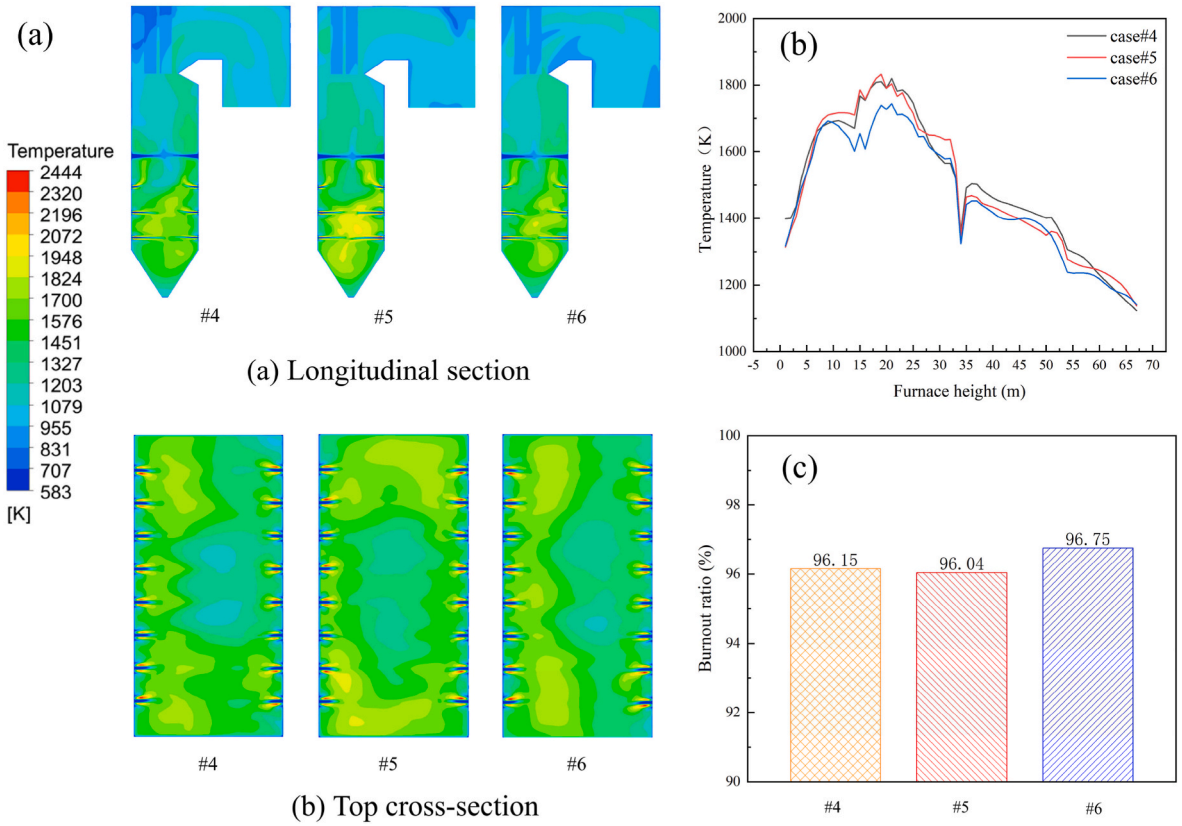

Fig. 11. (a) Temperature distribution contours, (b) temperature distribution along the furnace height and (c) burnout ration under I-type air distribution for different blended cases.

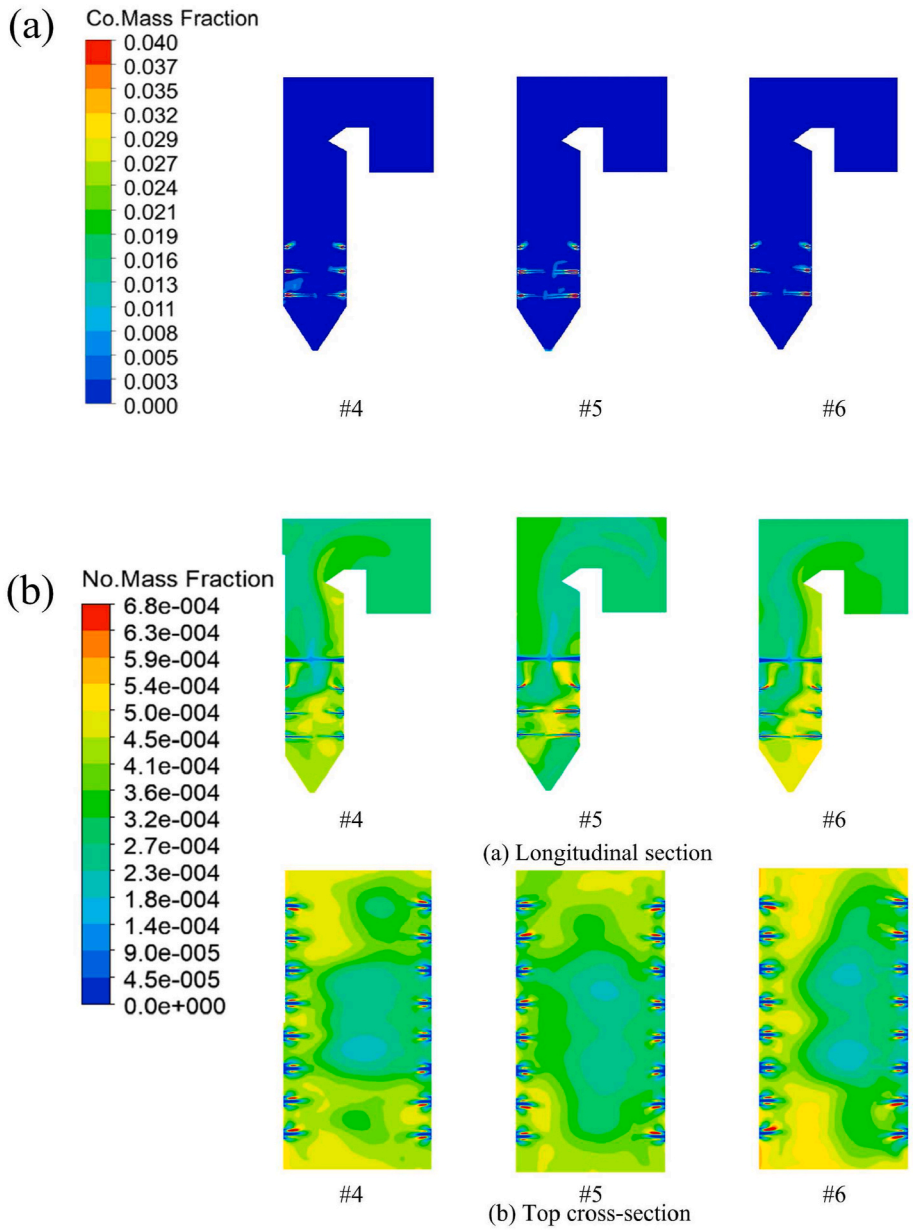

Fig. 12. CO concentration (a) and NO_x concentration (b) distribution under I-type air distribution for different blended cases.

case, and the reduced burnout rate results in wastage of fuel energy as well as reduced boiler efficiency.

NO_x production and reduction are related to the combustion characteristics of the fuel in the furnace, temperature variations, and component distribution. During combustion, nitrogen in the volatile fraction is primarily converted into nitrogen-containing intermediates such as HCN and NH_3. In the center of the furnace, these intermediates are oxidized to form NO, while in the fuel-rich region, the formed NO_x can be reduced back to N_2 [19]. In a low-NO_x swirl burner, the secondary air cyclone oxidizes HCN, NH_3, and char nitrogen to NO, and the uppermost OFA jet is injected to dilute the NO concentration in the flue gas to a lower level. Fig. 10 depicts the distribution contours of NO_x in the longitudinal and Top layer cross sections for different blending ratios. Although the temperature distribution of the furnace chamber and the trend of component concentration changes are similar in the four cases, there are still some differences in the NO_x production and reduction process. Since the set biomass is injected from the 3rd and 6th burners in each row, the NO_x concentration in the cross section will be concentrated in the center area. At 10% blending ratio, the NO_x concentration generated in the furnace is larger compared to case #0. As the blending ratio increases, the reducing atmosphere in the main combustion zone improves, and the NO_x concentration gradually decreases, reaching the lowest NO_x concentration in case #3 (30% blending ratio).

3.3. Combustion and pollutant emissions under different air distribution methods

3.3.1. I-type air distribution

Fig. 11(a) shows the temperature distribution contours in the longitudinal section of the furnace and the cross-section of the Top layer burner for increasing the mixing ratio from 10% to 30% under I-type air distribution conditions. Due to the average distribution of the air volume in each burner nozzle, the flame presents a flat front and the temperature distribution in the furnace is relatively uniform. Influenced by the flue gas flow in the Bottom and Mid layers, the high-temperature jet in the Top layer flows upward in the form of a semicircular sphere. The high-temperature flue gas region near the nozzle has a more pronounced

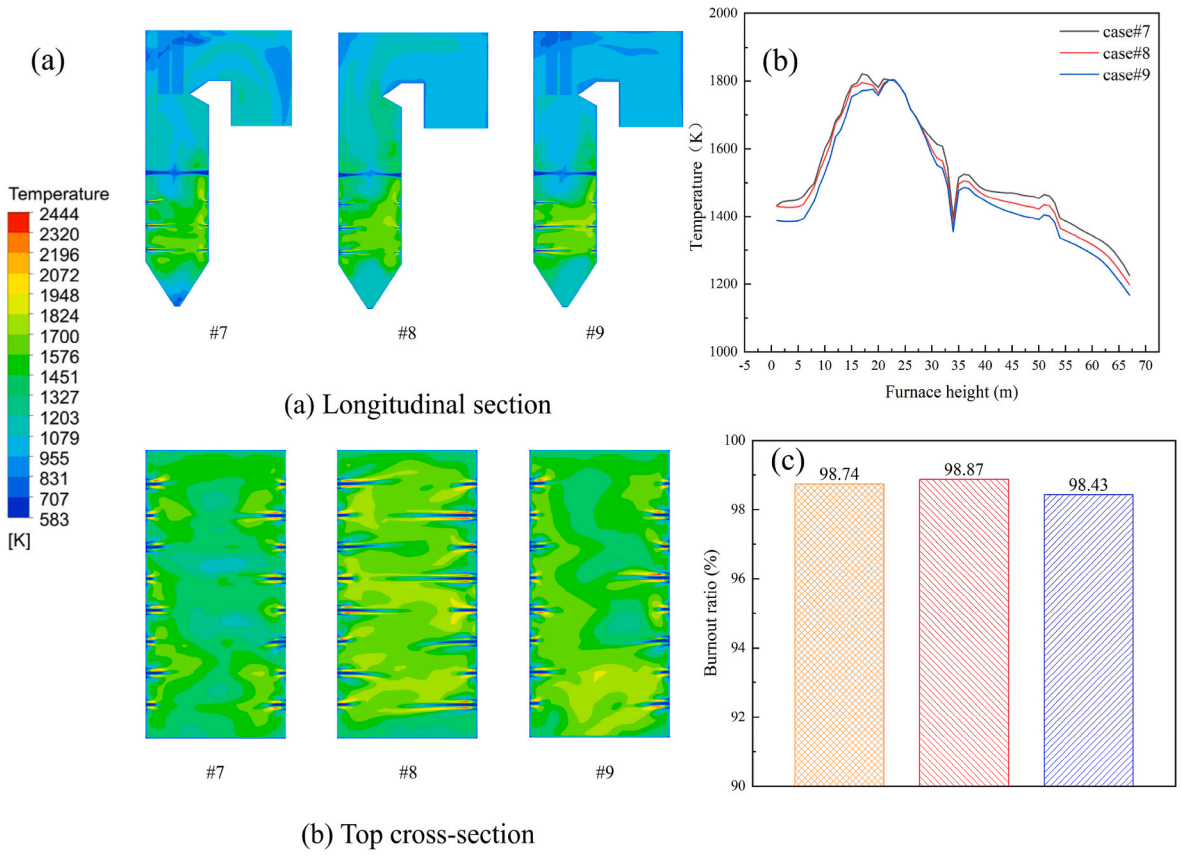

Fig. 13. (a) Temperature distribution contours, (b) temperature distribution along the furnace height and (c) burnout ration under W-type air distribution for different blended cases.

extension compared to the U-type air distribution. The phenomenon of wall-attached combustion to the side wall of the water wall in the combustion chamber is aggravated by the influence of the average air distribution, which is similar to the actual operation of the power station boiler. It can be observed that two agglomerated high temperature reflux flue gas zones appear on the left and right water wall sidewalls in case #5, which is significantly related to the upward flow of the lower flue gas. Fig. 11(b) illustrates the average temperature distribution along the height of the furnace for three different blending scenarios. In the combustion chamber region, there is a significant temperature gradient along the vertical direction, and different blending ratios exhibit significant temperature variations. It can be seen that #5 presents the highest average temperature. This is consistent with the conclusions of Gubba et al. [30]. When the blending ratio is increased to 30% (case #6), the average temperature of the chamber is lower compared to the other cases. This is the same conclusion as Li et al. [26] with a biomass mixture combustion ratio of 30%. In addition to the appearance of wall-attached combustion, the burnout rate is also a concern. As shown in Fig. 11(c), under the I-type air distribution, the combustion efficiency is generally higher than that of the U-type air distribution. The addition of biomass fuel in the operating conditions improves the combustion efficiency compared to the previous condition with pure coal powder. This indicates that this type of air distribution method helps to increase boiler efficiency.

Fig. 12(a) shows the CO concentration for different operating conditions under I-type air distribution. Under equal airflow conditions, fuels with different mixing ratios are fully combusted, and the CO concentration in the combustion chamber area does not vary much. Fig. 12 (b) illustrates the NO_x concentration distribution for different operating conditions under I-Type air distribution. The difference is that the NO_x concentration field under I-Type air distribution results in a distinct zone of low concentration at the burner level and a decrease in the cross-sectional average concentration. Compared to the U-type air distribution, the I-type air distribution reduces the air volume close to the burners on both sides, creating a zone of low O_2 concentration on both sides, which reduces the formation of NO_x. The increased airflow in the intermediate burner dilutes the concentration of NO_x, forming a central low-concentration zone. With an increase in the blending ratio, more eucalyptus wood replaces coal powder entering the boiler, thereby reducing the formation of fuel NO_x.The reduction of the furnace temperature correspondingly reduces the generation of thermal NO_x.

3.3.2. *W-type air distribution*

Fig. 13(a) illustrates the temperature distribution contours for different blending ratios under W-type air distribution. Compared with the previous two air distribution methods, the temperature distribution in the W-type air distribution furnace is more uniform, and the phenomenon of wall-attached combustion is also reduced. The high-temperature combustion zone is more concentrated in the combustion chamber. In the previous U-type and I-type air distribution methods, some fuel was still combusted in the cold ash hopper area. However, the W-type air distribution method increases turbulence between the same layer burners, forming more local eddies and increasing the combustion time of coal powder and eucalyptus wood in the furnace. As shown in Fig. 13(b), the average temperature distribution curve along the height of the furnace under W-type air distribution with different mixing ratios is depicted. Compared to the previous air distribution methods, it exhibits smaller temperature gradients. The average temperature fluctuations between different heights are also reduced. The smaller temperature gradients are beneficial in reducing the occurrence of tube bursting caused by uneven heating of the water wall. Additionally, the W-type air distribution also demonstrates improved combustion

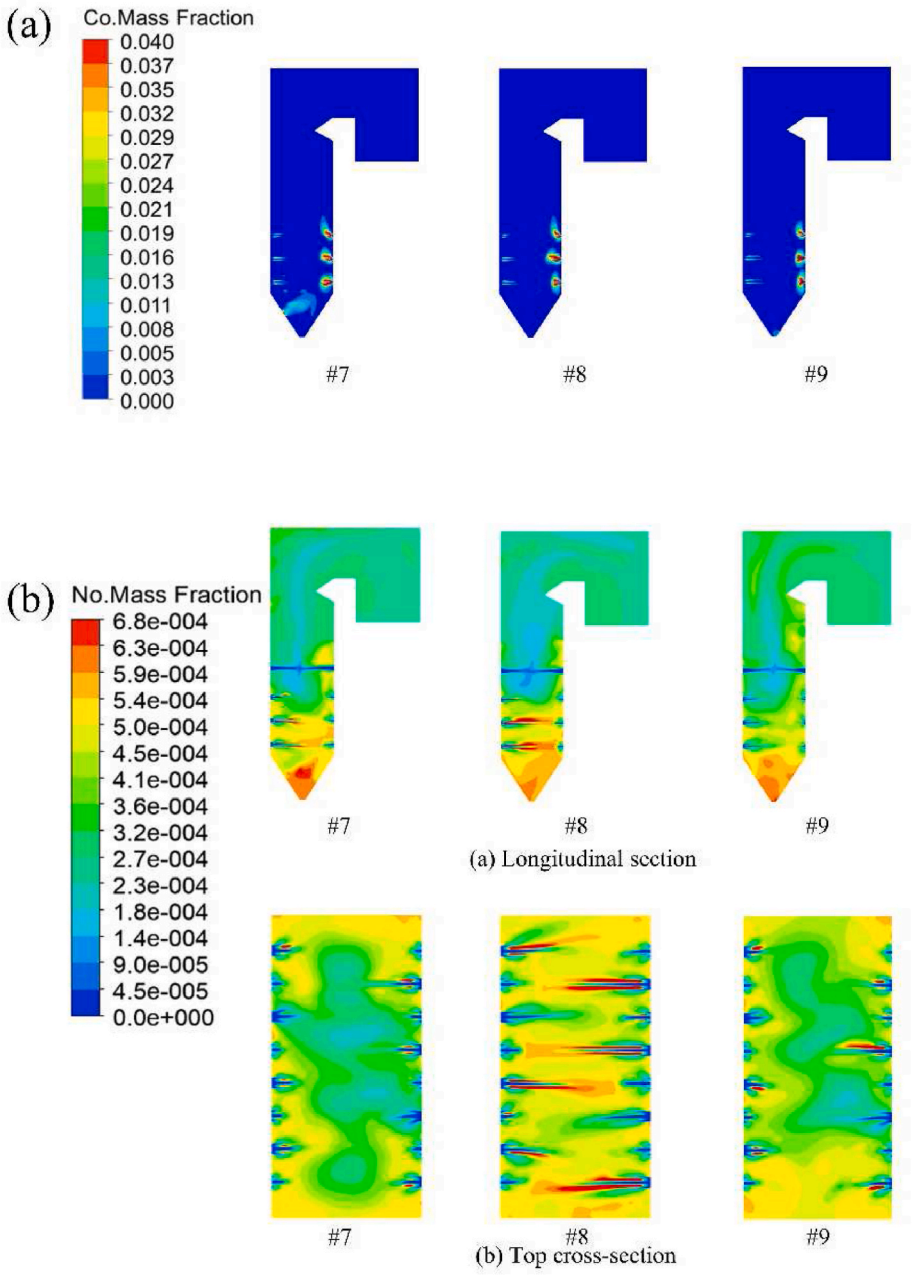

Fig. 14. CO concentration (a) and NO_x concentration (b) distribution under W-type air distribution for different blended cases.

efficiency. The W-type air distribution gets higher temperature in the combustion chamber region, increasing the fuel burnout rate, which is consistent with the conclusions of zhu et al. [31]· As shown in Fig. 13(c), each co-firing condition under this air distribution method achieves a combustion efficiency of over 98%. This can be attributed to the increased inter-layer turbulence, which extends the residence time of fuel particles and promotes more complete combustion. The increase in blending ratio has less effect on the burnout rate, so the W-type air distribution has a good generalization for blending biomass with different ratios.

Fig. 14(a) depicts the CO concentration for different blending ratios with W-type air distribution. The staggered air distribution further reduces the CO concentration, which is associated with an increase in the burnout rate. Fig. 14(b) illustrates the NO_x concentration distribution for different blending ratios under W-type air distribution. Compared with I-type air distribution, the W-type air distribution method shows more high concentration zones in the concentration distribution, especially located in the cold ash hopper part. It can be hypothesized that the cold ash hopper portion has a higher O_2 concentration due to the reduced residual carbon combustion, which decreases the reducing atmosphere in this region, thus increasing some of the NO_x production rates. It can be observed that the case with a blending ratio of 20% (case #8) obtains the highest NO_x concentration in the Top layer, and the fuller combustion of the fuel particles increases the production of fuel NO_x. Further increasing the blending ratio to the 30% condition (case #9) gives the lowest Top layer NO_x concentration. Eucalyptus wood contains less nitrogen than pulverized coal, and continuing to increase the blending ratio results in lower nitrogen content being brought into the boiler, which reduces the generation of fuel NO_x. At the same time eucalyptus wood has a lower low level calorific value than pulverized coal, and the lowered furnace temperature reduces the generation of thermal NO_x.

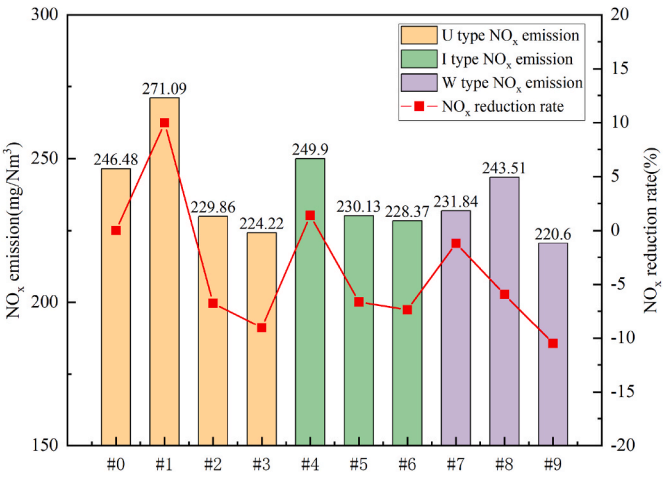

Fig. 15. The NO_x emission at the outlet and NO_x reduction rate.

3.4. NO_x emission and reduction rate for different air distribution and fuel blending ratio - a summary

As shown in Fig. 15, there are some differences in the NO_x concentration of the exit emission before when different air distribution methods and blending ratios are used. Compared to the original case #0, case #1 with 10% blending ratio increased the NO_x emission to 271.09 mg/Nm^3 at the outlet. The actual power plants typically have a blending ratio of 10%. As our simulation results have shown, using U-type air distribution at this blending ratio would result in an increase in the emission of gaseous pollutants. Comparing with case #1, cases #4 and #7 show better NO_x emission reduction at the same 10% mixing ratio. Among them, case #7 exhibits the best performance, with NOx emissions reduced to 231.84 mg/Nm^3 at the outlet. This indicates that the W-type air distribution method is more effective in both inhibiting and reducing the generation of NO_x at lower co-firing rates. The study of wang et al. [32] also showed that staggered airflow distribution can better suppress NOx production. However, the same approach does not work for a blending ratio of 20%, and it can be observed that for cases #2, #5, and #8, a higher NO_x emission is obtained with the W-type air distribution (#8). In contrast, NO_x emissions were reduced to 229.86 mg/Nm^3 and 230.13 mg/Nm^3 using U-type air distribution (#2) and I-type air distribution (#5), respectively. Considering the side-wall-attached combustion phenomenon that occurs in case #5, the U-type air distribution is a more suitable air distribution for the 20% blending ratio when there is not much difference in the burnout rate. For higher blending (30% blending ratio), case #3, #6, and #9 al l show satisfactory emission reduction. It is worth noting that in all simulated scenarios, condition #9 exhibits the lowest NO_x emissions. It successfully controls the NO_x emission concentration at the boiler outlet to 220.6 mg/Nm^3, while also achieving the highest combustion efficiency among the three air distribution methods. The simulation results show that different air distribution methods and blending ratios have certain effects on the NO_x concentration at the boiler outlet. The optimal air distribution method can be selected based on different blending ratios, and adjustments can also be made to the operation of the boiler by considering parameters such as temperature distribution and combustion completeness. This is of practical significance for the optimization of ultra-supercritical coal-fired boilers and biomass co-firing.

4. Conclusion

In this study, numerical simulation is used to investigate the co-firing process of pulverized coal and eucalyptus wood in a 1000MWth opposed wall-fired boiler under different air distribution methods. The combustion efficiency and NO_x emissions of coal under different air distribution methods and different blending ratios of eucalyptus are discussed, leading to the following conclusions:

1) According to the simulation results based on the original U-type air distribution method of the power plant boiler, it is found that under a blending ratio of 10%, the degree of erosion caused by fuel particles on the screen-type superheater is the lowest. However, as the blending ratio increases, the erosion degree also increases. This increase in erosion corresponds with a decrease in combustion efficiency, which reached a minimum value of 93.86%.
2) The burnout rate of the boiler is further improved by applying the I-type air distribution method, but the simulation results show that the flame has a serious wall-attached phenomenon. After changing the air distribution method to W-type, the combustion rate reaches the highest value of the three air distribution methods, and the problem of large fluctuation of combustion rate under different blending ratios is also solved, and the phenomenon of wall-attached combustion is also solved.
3) For NO_x emission reduction, the optimum air distribution method varies for different blending ratios. At 10% blending ratio, the lowest NO_x emission (231.84 mg/Nm^3) can be obtained by using W-type air distribution (case #7). The U-type and I-type air distribution methods show equal inhibition of NO_x generation at a mixing ratio of 20%, with outlet concentrations of 229.86 mg/Nm^3 and 230.13 mg/Nm^3, respectively. However, case #5 has a higher burnout rate (96.04%) than case #2 and is the optimal combustion case for this blending ratio. Case #9 (30% blending ratio) has the highest burnout rate in the furnace and the lowest NO_x emission at the outlet (220.6mg/Nm^3).

CRediT authorship contribution statement

Junxuan Huang: Writing – review & editing, Writing – original draft, Visualization, Validation, Software, Methodology, Investigation, Formal analysis, Data curation, Conceptualization. **Yanfen Liao:** Writing – review & editing, Funding acquisition, Conceptualization. **Jianhua Lin:** Supervision, Resources, Methodology. **Changjiang Dou:** Supervision, Resources, Methodology. **Zengxiu Huang:** Supervision, Resources, Methodology. **Xiongwei Yu:** Supervision, Resources, Methodology. **Zhaosheng Yu:** Supervision, Resources, Methodology. **Chunxiang Chen:** Supervision, Resources, Methodology. **Xiaoqian Ma:** Supervision, Resources, Conceptualization.

Declaration of competing interest

The authors declare that they have no known competing financial interests or personal relationships that could have appeared to influence the work reported in this paper.

Data availability

Data will be made available on request.

Acknowledgments

This work was supported by the Guangxi Key Research and Development Natural Science Foundation (GUIKEAB22035033) and the Fundamental Research Funds for the Central Universities (2022ZFJH04).

Appendix A. Supplementary data

Supplementary data to this article can be found online at https://doi.org/10.1016/j.energy.2024.131306.

References

[1] Forster PM, Smith CJ, Walsh T, Lamb WF, Lamboll R, Hauser M, et al. Indicators of Global Climate Change 2022: annual update of large-scale indicators of the state of the climate system and human influence. Earth Syst Sci Data 2023;15:2295–327. https://doi.org/10.5194/essd-15-2295-2023.

[2] Agbor E, Zhang X, Kumar A. A review of biomass co-firing in North America. Renew Sustain Energy Rev 2014;40:930–43. https://doi.org/10.1016/j.rser.2014.07.195.

[3] De Laporte AV, Weersink AJ, McKenney DW. Effects of supply chain structure and biomass prices on bioenergy feedstock supply. Appl Energy 2016;183:1053–64. https://doi.org/10.1016/j.apenergy.2016.09.049.

[4] Mohd Idris MN, Hashim H, Razak NH. Spatial optimisation of oil palm biomass co-firing for emissions reduction in coal-fired power plant. J Clean Prod 2018;172:3428–47. https://doi.org/10.1016/j.jclepro.2017.11.027.

[5] Savolainen K. Co-firing of biomass in coal-fired utility boilers. Appl Energy 2003;74:369–81. https://doi.org/10.1016/S0306-2619(02)00193-9.

[6] Steer J, Marsh R, Griffiths A, Malmgren A, Riley G. Biomass co-firing trials on a down-fired utility boiler. Energy Convers Manag 2013;66:285–94. https://doi.org/10.1016/j.enconman.2012.10.010.

[7] Oladejo JM, Adegbite S, Pang CH, Liu H, Parvez AM, Wu T. A novel index for the study of synergistic effects during the co-processing of coal and biomass. Appl Energy 2017;188:215–25. https://doi.org/10.1016/j.apenergy.2016.12.005.

[8] Wu D, Wang Y, Wang Y, Li S, Wei X. Release of alkali metals during co-firing biomass and coal. Renew Energy 2016;96:91–7. https://doi.org/10.1016/j.renene.2016.04.047.

[9] Tu Y, Li J, Chang D, Hu B. Effect of biomass co-firing position on combustion and NO $_{X}$ emission in a 300-MWe coal-fired tangential boiler. Asia Pac J Chem Eng 2022;17. https://doi.org/10.1002/apj.2734.

[10] Mun T-Y, Tumsa TZ, Lee U, Yang W. Performance evaluation of co-firing various kinds of biomass with low rank coals in a 500 MWe coal-fired power plant. Energy 2016;115:954–62. https://doi.org/10.1016/j.energy.2016.09.060.

[11] Wei Y, Li D, Qiao J, Guo X. Recovery of spent SCR denitration catalyst: a review and recent advances. J Environ Chem Eng 2023;11:110104. https://doi.org/10.1016/j.jece.2023.110104.

[12] Wang D, Luo J, Yang Q, Yan J, Zhang K, Zhang W, et al. Deactivation mechanism of multipoisons in cement furnace flue gas on selective catalytic reduction catalysts. Environ Sci Technol 2019;53:6937–44. https://doi.org/10.1021/acs.est.9b00337.

[13] Ti S, Chen Z, Kuang M, Li Z, Zhu Q, Zhang H, et al. Numerical simulation of the combustion characteristics and NO emission of a swirl burner: influence of the structure of the burner outlet. Appl Therm Eng 2016;104:565–76. https://doi.org/10.1016/j.applthermaleng.2016.05.079.

[14] Nemitallah MA, Habib MA, Badr HM, Said SA, Jamal A, Ben-Mansour R, et al. Oxy-fuel combustion technology: current status, applications, and trends. Int J Energy Res 2017;41:1670–708. https://doi.org/10.1002/er.3722.

[15] Qi X, Ma X, Yu Z, Huang Z, Teng W. Numerical simulation of municipal waste and food digestate blending combustion and NOx reduction under oxygen-enriched atmospheres. Fuel 2023;345:128115. https://doi.org/10.1016/j.fuel.2023.128115.

[16] Zhu T, Hu Y, Tang C, Wang L, Liu X, Deng L, et al. Experimental study on NO formation and burnout characteristics of pulverized coal in oxygen enriched and deep-staging combustion. Fuel 2020;272:117639. https://doi.org/10.1016/j.fuel.2020.117639.

[17] Hou S-S, Chiang C-Y, Lin T-H. Oxy-fuel combustion characteristics of pulverized coal under O2/recirculated flue gas atmospheres. Appl Sci 2020;10:1362. https://doi.org/10.3390/app10041362.

[18] Wang Y, Zhou Y, Bai N, Han J. Experimental investigation of the characteristics of NOx emissions with multiple deep air-staged combustion of lean coal. Fuel 2020;280:118416. https://doi.org/10.1016/j.fuel.2020.118416.

[19] Wang Y, Zhou Y. Numerical optimization of the influence of multiple deep air-staged combustion on the NOx emission in an opposed firing utility boiler using lean coal. Fuel 2020;269. https://doi.org/10.1016/j.fuel.2019.116996.

[20] Sung Y, Moon C, Eom S, Choi G, Kim D. Coal-particle size effects on NO reduction and burnout characteristics with air-staged combustion in a pulverized coal-fired furnace. Fuel 2016;182:558–67. https://doi.org/10.1016/j.fuel.2016.05.122.

[21] Zhang W, Pei J, Zhu Z, Ye Z, You C. Optimization of the Combustion Organization in a 1000 MW $_{e}$ Opposed Wall-Fired Utility Boiler by Wall Air Injection. Combust Sci Technol 2022:1–17. https://doi.org/10.1080/00102202.2022.2097007.

[22] Tabet F, Gökalp I. Review on CFD based models for co-firing coal and biomass. Renew Sustain Energy Rev 2015;51:1101–14. https://doi.org/10.1016/j.rser.2015.07.045.

[23] Gómez MA, Porteiro J, de la Cuesta D, Patiño D, Míguez JL. Numerical simulation of the combustion process of a pellet-drop-feed boiler. Fuel 2016;184:987–99. https://doi.org/10.1016/j.fuel.2015.11.082.

[24] Benim AC, Deniz Canal C, Boke YE. Computational investigation of oxy-combustion of pulverized coal and biomass in a swirl burner. Energy 2022;238. https://doi.org/10.1016/j.energy.2021.121852.

[25] Zhong BJ, Roslyakov PV. Study on prompt NOx emission in boilers. J Therm Sci 1996;5:143–7. https://doi.org/10.1007/s11630-996-0013-y.

[26] Li D, Lv Q, Feng Y, Wang C, Liu X, Du Y, et al. Numerical study of Co-firing biomass with lean coal under air-fuel and oxy-fuel conditions in a wall-fired utility boiler. Energy Fuel 2017;31:5344–54. https://doi.org/10.1021/acs.energyfuels.7b00207.

[27] Wei L, Zhou Q, Li N. Experimental study and simulation analysis of heat and deformation in the water walls of an opposed firing boiler under flexible operating conditions. Appl Therm Eng 2022;213:118726. https://doi.org/10.1016/j.applthermaleng.2022.118726.

[28] Gao R, Yin S, Song T, Lu P. Numerical simulation of co-combustion of pulverized coal and biomass in TTF precalciner. Fuel 2023;334. https://doi.org/10.1016/j.fuel.2022.126515.

[29] Kim G-M, Choi JH, Jeon C-H, Lim D-H. Effects of cofiring coal and biomass fuel on the pulverized coal injection combustion zone in blast furnaces. Energies 2022;15:655. https://doi.org/10.3390/en15020655.

[30] Gubba SR, Ingham DB, Larsen KJ, Ma L, Pourkashanian M, Tan HZ, et al. Numerical modelling of the co-firing of pulverised coal and straw in a 300 MWe tangentially fired boiler. Fuel Process Technol 2012;104:181–8. https://doi.org/10.1016/j.fuproc.2012.05.011.

[31] Zhu T, Hu Y, Tang C, Wang L, Liu X, Deng L, et al. Experimental study on NOx formation and burnout characteristics of pulverized coal in oxygen enriched and deep-staging combustion. Fuel 2020;272. https://doi.org/10.1016/j.fuel.2020.117639.

[32] Wang C, Chen M, Zhao P, Zhou L, Hou Y, Zhang J, et al. Investigation on Co-combustion characteristics and NOx emissions of coal and municipal sludge in a tangentially fired boiler. Fuel 2023;340. https://doi.org/10.1016/j.fuel.2023.127608.